remote sensing

MDPI

Article

Electrical Structure of Southwestern Longmenshan Fault Zone: Insights into Seismogenic Structure of 2013 and 2022 Lushan Earthquakes

Yan Zhan [1], Xiangyu Sun [1], Guoze Zhao [1,*], Lingqiang Zhao [2], Xiaoping Yang [1], Haibo Yang [1], Dawei Jiang [3] and Xiaoyu Lou [1]

[1] State Key Laboratory of Earthquake Dynamics, Institute of Geology, China Earthquake Administration, Beijing 100029, China; zhanyan@ies.ac.cn (Y.Z.); sunxiangyu@ies.ac.cn (X.S.); xpyang@ies.ac.cn (X.Y.); yanghaibo2015@ies.ac.cn (H.Y.); louxiaoyu@ies.ac.cn (X.L.)
[2] Second Monitoring and Application Center, China Earthquake Administration, Xi'an 710054, China; zhaolingqiang0926@126.com
[3] National Institute of Natural Hazards, Ministry of Emergency Management of China, Beijing 100085, China; daweijiang@ninhm.ac.cn
* Correspondence: zhaogz@ies.ac.cn

Abstract: On 1 June 2022, a magnitude 6.1 earthquake struck the southern segment of the Longmenshan fault zone on the eastern edge of the Tibetan Plateau, once again causing casualties and economic losses. Understanding the deep-seated dynamic mechanisms that lead to seismic events in the Lushan earthquake area and assessing the potential hazards in seismic gap areas are of significant importance. In this study, we utilized 118 magnetotelluric datasets collected from the Lushan earthquake area and employed three-dimensional electromagnetic inversion with topographic considerations to characterize the deep-seated three-dimensional resistivity structure of the Lushan earthquake area. The results reveal that the Shuangshi–Dachuan fault in the Lushan earthquake area can be divided into two relatively low-resistivity zones: a western zone dipping southeastward and an eastern zone with a steeper slightly northwestern dip. These two zones intersect at a depth of approximately 20 km, forming an extensional pattern resembling a "Y" shape. The epicenters of both the 2013 and 2022 Lushan earthquakes are primarily located in the upper constricted portion of the pocket-like low-resistivity body at depth. The distribution of seismic aftershocks is confined within the region enclosed by the high-resistivity body, following the pattern of the Y-shaped low-resistivity zone.

Keywords: Lushan earthquake; Longmenshan fault zone; Sichuan Basin; magnetotelluric

Citation: Zhan, Y.; Sun, X.; Zhao, G.; Zhao, L.; Yang, X.; Yang, H.; Jiang, D.; Lou, X. Electrical Structure of Southwestern Longmenshan Fault Zone: Insights into Seismogenic Structure of 2013 and 2022 Lushan Earthquakes. *Remote Sens.* **2024**, *16*, 370. https://doi.org/10.3390/rs16020370

Academic Editors: Gianluca Groppelli, Kejie Chen, Wanpeng Feng, Dun Wang and Lihua Fang

Received: 31 October 2023
Revised: 27 December 2023
Accepted: 31 December 2023
Published: 17 January 2024

1. Introduction

The Longmenshan fault zone (LMSFZ) is a well-known thrust fault located on the eastern edge of the Tibetan Plateau (Figure 1). This fault marks the boundary between the highly active Tibetan Plateau and the stable Sichuan Basin, extending for a length of approximately 500 km [1–3]. The LMSFZ is also situated in the central part of the North–South seismic belt in China, making it one of the most seismically active regions in mainland China in recent years. Based on criteria such as fault activity, seismic distribution, and rupture modes during earthquakes at various locations along the LMSFZ, it can be subdivided into different segments. While there is some controversy regarding the exact boundaries between these segments, they can generally be categorized as the northeastern segment, central segment, and southwestern segment [4].

One of the most notable earthquakes to occur along the LMSFZ was the 2008 Wenchuan Ms8.0 earthquake, which struck the central segment. This earthquake was the second-largest in magnitude to occur in mainland China since the beginning of the century and resulted in significant human casualties and property damage [5]. Prior to the Wenchuan

earthquake, the LMSFZ had experienced a long period of seismic quiescence. This led to underestimation of the seismic hazard associated with the LMSFZ [6]. Surface ruptures during the Wenchuan earthquake propagated along the LMSFZ in a northeastward direction [5,7,8], while the southwestern segment of the fault remained inactive during the event [6,9]. The occurrence of the Wenchuan Ms8.0 earthquake highlighted the high seismic hazard potential associated with previously creeping faults [10].

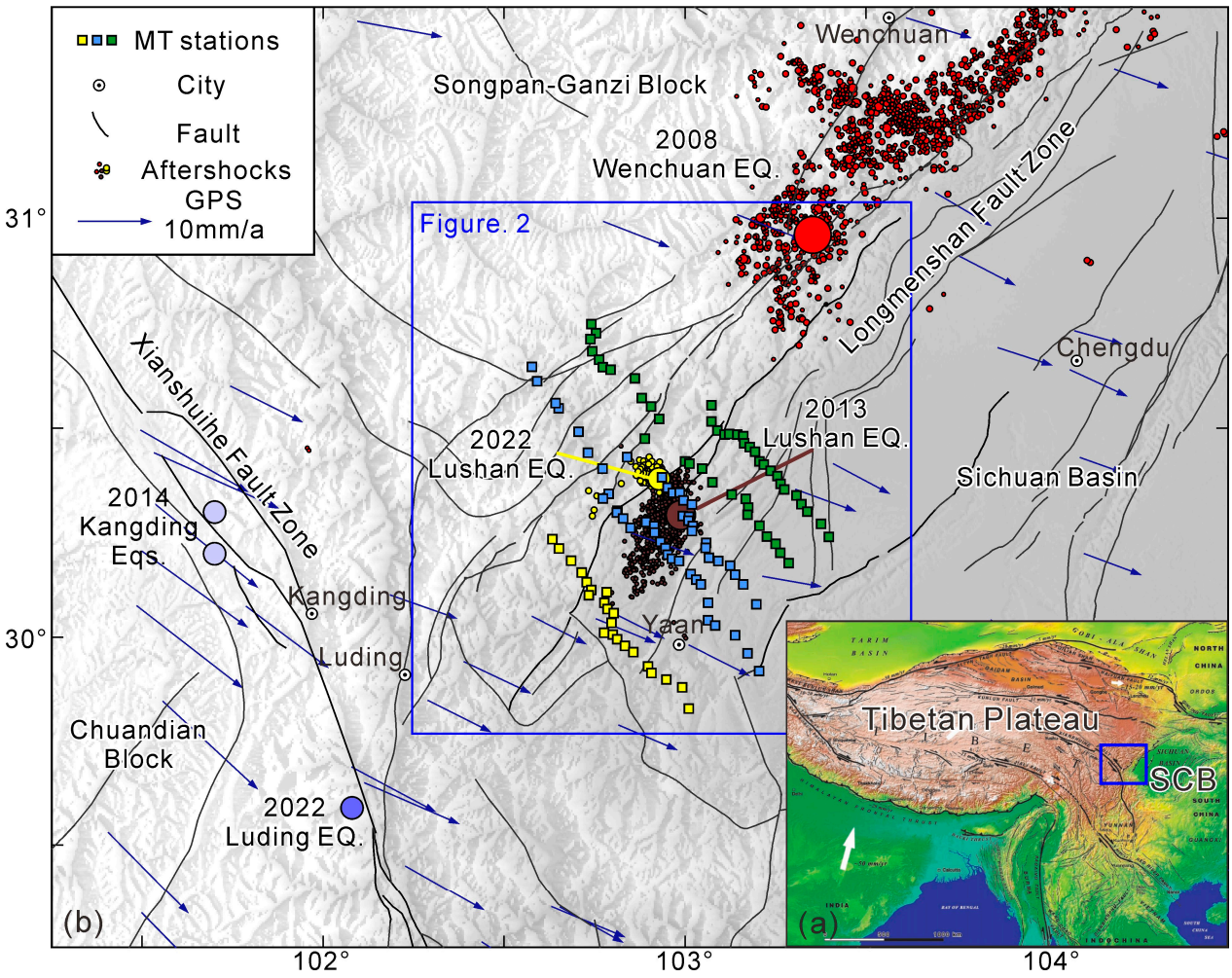

Figure 1. (**a**) Location of the study region [11]. (**b**) Map showing locations of MT stations, faults, and earthquakes. Circles denote mainshocks and aftershocks [12–14]. Squares denote MT stations. Abbreviations are EQ, earthquake; SCB, Sichuan Basin.

Despite some studies indicating that the Wenchuan earthquake released accumulated strain along the LMSFZ [15], another earthquake occurred on this fault five years later. The 2013 Lushan M7.0 earthquake struck the southwestern segment of the LMSFZ, approximately 100 km from the epicenter of the Wenchuan earthquake (Figure 2). Geological surveys conducted after the Lushan earthquake did not reveal any surface rupture [16]. Deep seismic results suggested that the 2013 Lushan earthquake was caused by the activation of a buried thrust fault [17]. Locations of aftershocks revealed that the fault plane of the 2013 Lushan earthquake dipped northwestward, with a steep shallow angle and a gentler angle at greater depths, displaying characteristics of a "shovel-shaped" thrust fault. Additionally, a southeast-dipping aftershock zone intersected with the deep-seated fault in the east, forming a "Y" shape [13,14]. In 2022, another earthquake with a magnitude of 6.1 occurred in Lushan County. The relocated epicenters of the mainshock and aftershocks indicated an initial rupture depth of 18.9 km for the mainshock, with the aftershocks con-

centrated at depths between 11 and 19 km. The epicenters clustered within an elliptical area approximately 8 km long in the northeast–southwest direction and 6 km wide in the northwest–southeast direction [18]. Remarkably, the epicenters of these two Lushan earthquakes were only 8 km apart.

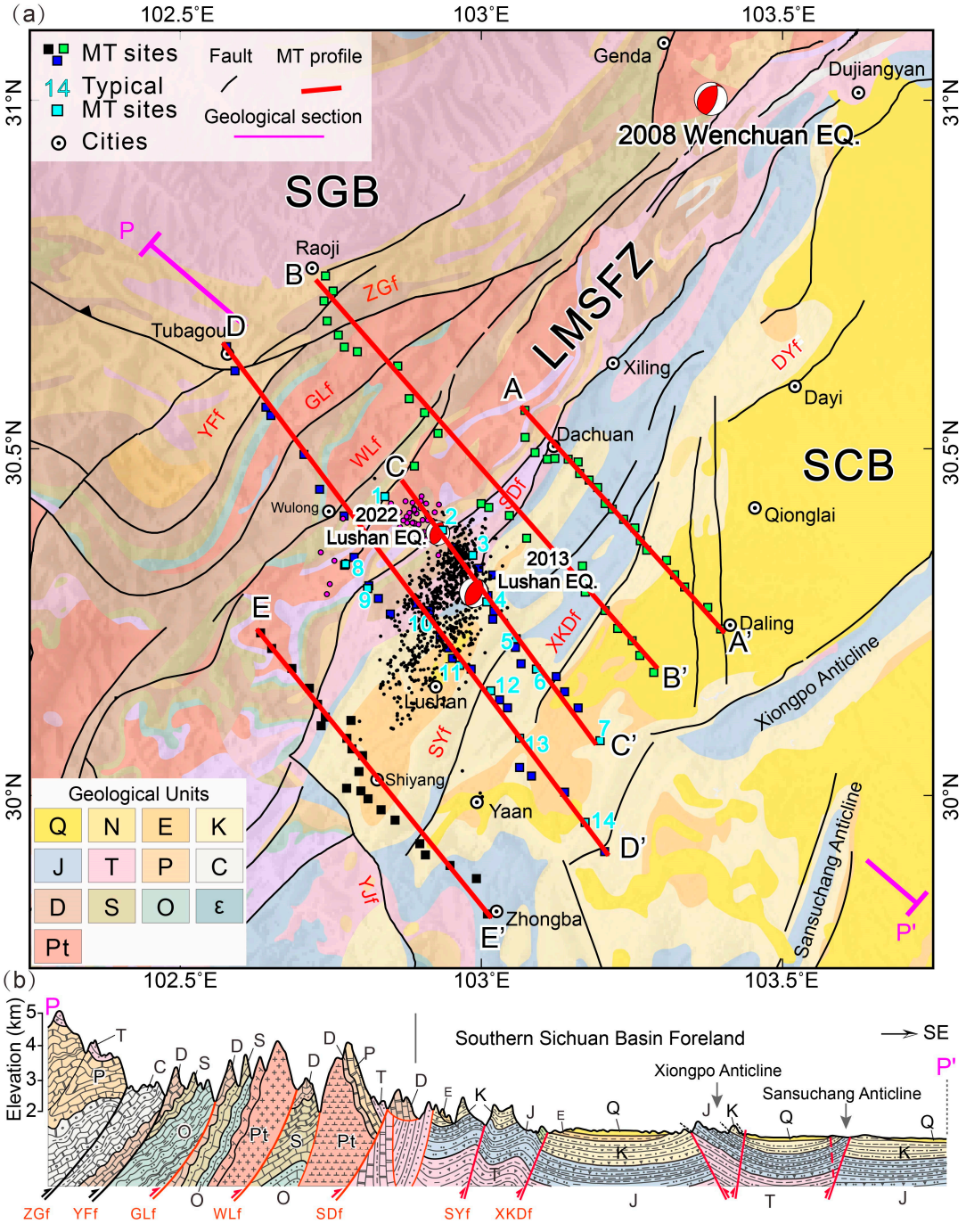

Figure 2. (**a**) Geology map of the Lushan earthquakes region. (**b**) Geological section of the Lushan earthquakes region [19]. Abbreviations are LMSFZ, Longmenshan fault zone; SCB, Sichuan Basin; SGB, Songpan–Ganzi block; ZGf, Zhonggang fault; YFf, Yongfu fault; GLf, Gengda–Longdong fault; WLf, Wulong fault; SDf, Shuangshi–Dachuan fault; SYf, Shouyang fault; XKDf, Xinkaidian fault; DYf, Dayi fault.

Following the 2013 Lushan earthquake, various research efforts have been carried out in the region. For instance, receiver function studies have shown that the LMSFZ serves as

a transition zone between the Songpan–Ganzi block and the Sichuan Basin, with significant Moho discontinuity deformation or segmentation [20]. Deep reflection profile studies revealed the existence of Y-shaped or flower-like fault combinations within the crust in the Lushan earthquake area [21,22]. However, these studies were limited to a single profile and lacked three-dimensional coverage, making it challenging to effectively constrain the complex structural features in the Lushan earthquake area. P-wave receiver functions results reveal that there are substantial differences in crustal lithospheric structures between the Songpan–Ganzi block, the LMSFZ, and the Sichuan Basin [23]. Nevertheless, their study also relied on a single profile crossing the Lushan earthquake area. A seismic array was used to investigate the velocity structures and fault geometry in the seismic gap area, but an in-depth analysis of the crustal fine structure in the Lushan earthquake area was not performed [24,25]. Velocity structures for different periods along the LMSFZ indicated that the Lushan earthquake area exhibits faster healing compared to the Wenchuan earthquake area [26].

The magnetotelluric (MT) method enables the acquisition of a subsurface electrical structure, exhibiting sensitivity to underground fluids and high-temperature materials. Several studies suggest that the presence of fluids plays a crucial role in seismic generation and nucleation mechanisms [27–31]. Therefore, investigating subsurface electrical structures contributes to a better understanding of the deep-seated seismogenic environment in the LMSFZ and provides essential insights for assessing future earthquake risks along the LMSFZ. After the 2013 Lushan earthquake, multiple MT profiles traversing the earthquake area were employed to study the crustal structure [32–35]. However, the electrical structure was derived using 2D inversion, limiting its ability to investigate variations in electrical structure along the profiles. In a recent study, three-dimensional inversion of magnetotelluric data was conducted in the Lushan earthquake area, obtaining the first 3D electrical structure of the region [36]. The results indicated that both earthquakes occurred within the same highly conductive body, thus categorizing the 2022 Lushan earthquake as a strong aftershock of the 2013 Lushan earthquake. While this study aimed for as even coverage of data points as possible across both Lushan earthquake areas [36], it is evident that more densely distributed data are required to unveil the deep structural characteristics of the numerous northeast trending faults in the region and gain a deeper understanding of the seismogenic environment of the two Lushan earthquakes.

2. Data Analysis

The southwestern segment of the LMSFZ is situated in a region characterized by the convergence of multiple tectonic units. It features rugged terrain, a dense network of power lines, numerous mining areas, and hydropower stations, making fieldwork challenging and data acquisition demanding. In the months of May and June 2013, we conducted magnetotelluric measurements in the southwestern segment of the LMSFZ. In this area, a total of 118 MT stations were collected along five profiles. Previous studies performed two-dimensional inversions and conducted underground structure interpretations and research based on three of these profiles [33,35]. This paper incorporates data from these three profiles along with data from two additional profiles.

Figure 3 presents apparent resistivity and impedance phase curves for 14 representative MT stations(highlighted as light blue squares in Figure 2) along the CC′ and DD′ profiles. Stations 1 and 2, as well as 8 and 9, cross the Shuangshi–Dachuan fault (SDf) and exhibit distinct electrical discontinuities. To the northwest of this fault zone, the apparent resistivity values within the LMSFZ are relatively high, while, on the southeast side, apparent resistivity values for all MT stations generally decrease below several hundred ohm-meters. However, the shapes of these curves vary, reflecting the deep-seated complexity at the interface between the LMSFZ and the Sichuan Basin. MT stations in proximity to the western (SDf1) and eastern (SDf2) branches of the Shuangshi–Dachuan fault show notably lower apparent resistivity values compared to stations on either side. Beneath the fault zone, there are electrical discontinuities, and MT stations on the southeastern side of the

Lushan earthquake area consistently exhibit low-resistivity characteristics in the longer periods, indicating the presence of a deeper low-resistivity layer.

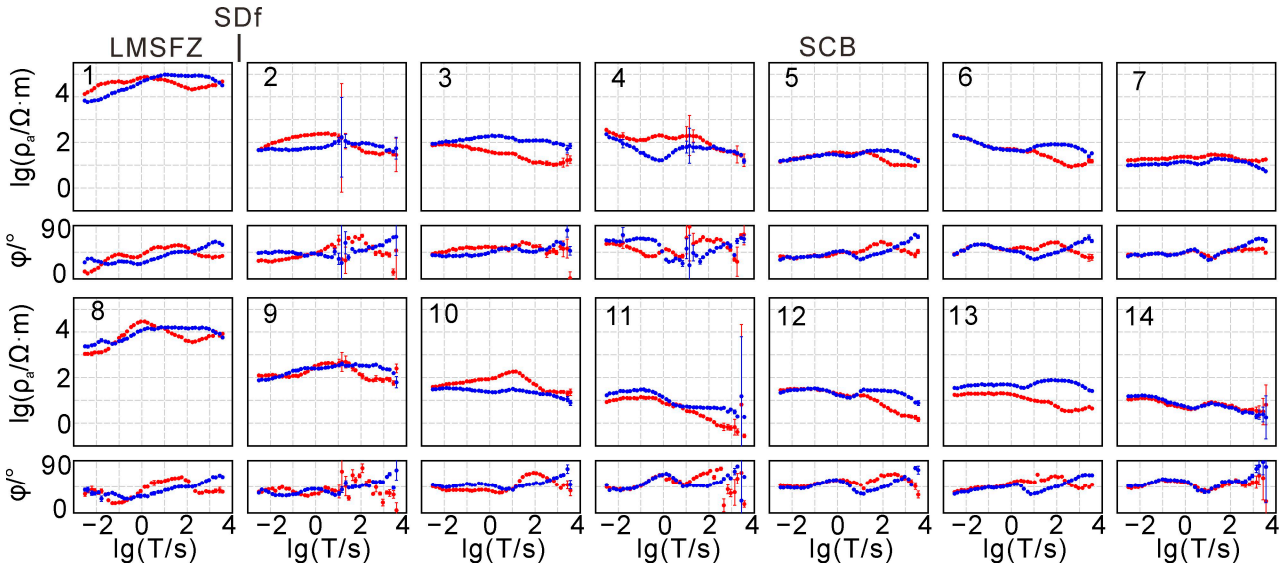

Figure 3. Apparent resistivity and phase curves for typical MT sites (see Figure 2 for the locations). Red points denote data in XY direction, blue points denote data in YX direction.

The two-dimensional skew β, obtained from phase tensor [37,38], can be employed to assess the anisotropy of the subsurface medium. Considering that observational data inherently contain some level of error, it is generally considered that β values exceeding 3 indicate a significant level of three-dimensionality in the subsurface structure [39,40]. Figure 4 illustrates the distribution of β values for four different periods. MT stations in the vicinity of the Shuangshi–Dachuan fault, as well as those within the LMSFZ on both sides, exhibit β values exceeding 3 in the high-frequency range. Notably, in the vicinity of the Shuangshi–Dachuan fault, especially in the epicentral region of the Lushan earthquake, β values significantly exceed 3 at periods ranging from approximately 10 s to several tens of seconds. This indicates that the deeper structures exhibit typical three-dimensional features. Therefore, obtaining a more accurate depiction of the deep electrical structure necessitates the utilization of three-dimensional electromagnetic imaging inversion techniques.

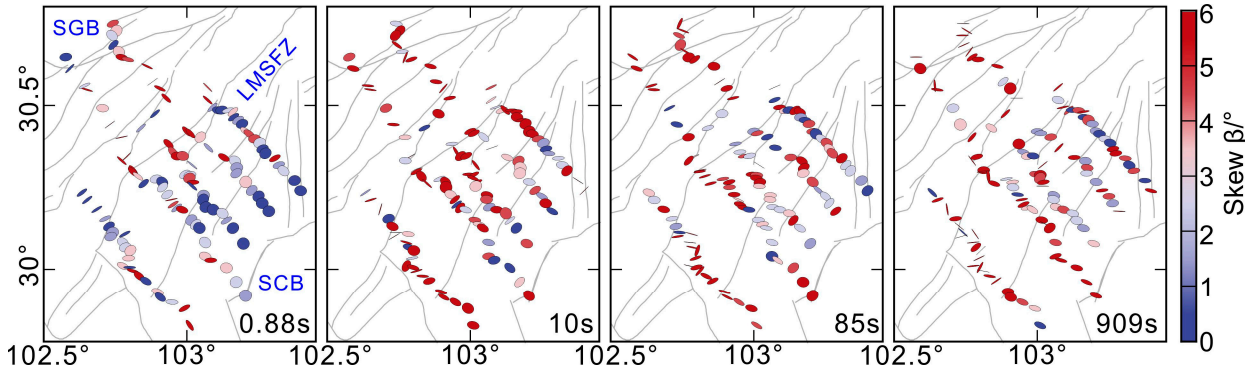

Figure 4. Phase tensor ellipses filled with the skew angle β.

3. 3D Inversion and Results

Ideally, for three-dimensional inversion to best recover subsurface structures, a uniform distribution of MT stations and the utilization of all the components of the magnetotelluric transfer function are preferred. However, practical considerations such as transportation constraints, topographical variations, and other factors often result in un-

evenly distributed MT stations. In some cases, datasets are organized in profiles [41]. It has been demonstrated that three-dimensional inversion of such datasets can provide more accurate subsurface structural information compared to two-dimensional inversion [42]. The dataset used in this study is distributed along five MT profiles. Due to the complex structural nature of the region and the strong three-dimensionality revealed by the phase tensor analysis, the decision was made to employ three-dimensional inversion to characterize the deep structures in the area. The three-dimensional inversion was conducted using ModEM [43,44].

Given the high population density and the presence of numerous hydroelectric power stations in the region, the quality of the diagonal elements of the data is relatively poor. As a result, the inversion process utilized apparent resistivity and impedance phase data from the off-diagonal elements. A total of 118 MT stations were incorporated in the inversion, covering a period range from 0.00325 s to 7300 s. Throughout the inversion process, an error floor of 10% was applied to the apparent resistivity data, while a 5% error floor was applied to the impedance phase data. In terms of error propagation, this is equivalent to introducing a 5% error into the impedance data.

The central part of the three-dimensional inversion model has a grid size of 1.5 km × 1.5 km, with a total of 74 × 58 grids. Beyond the central area, there are an additional 10 expansion grids in each direction, increasing the grid spacing by a factor of 1.5, resulting in a final grid count of 94 × 78. The southwestern segment of the LMSFZ experiences significant topographical variations, and these variations needed to be considered during the inversion process. The model consists of a total of 164 vertical layers, including 86 layers with a thickness of 50 m and 78 layers with gradually increasing thickness from 50 m (Figure 5). Based on DEM data for the study area (Figure 1), grid cells above Earth's surface were designated as air cells and were kept unchanged throughout the inversion process.

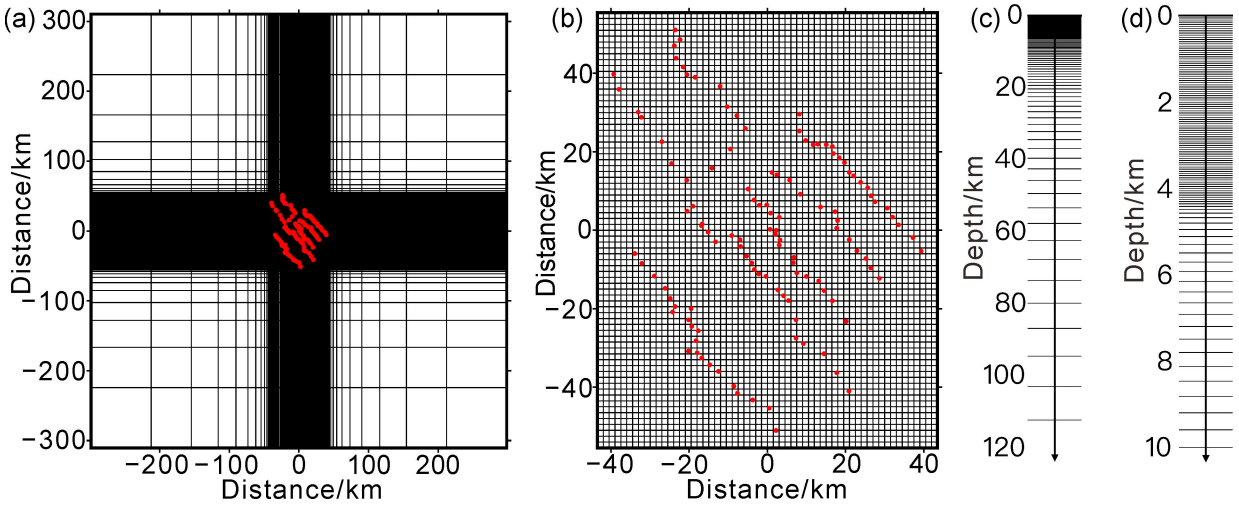

Figure 5. (**a**) Horizontal grid for the 3D inversion model. (**b**) Central part of the horizontal grid. (**c**) Vertical grids within the depth of 120 km. (**d**) Vertical grids within the depth of 10 km. Red dots denote MT stations.

The initial resistivity of the three-dimensional inversion model was set to 100 Ωm based on the average apparent resistivity of the MT stations. The smoothing factors in all three directions were set to 0.2. An automatic updating regularization factor was applied, with an initial value of 5000. When the inversion no longer converged, the regularization factor was reduced to one-tenth of its original value. The final fitting root mean square (RMS) error was 2.05 (as shown in Figure 6). The fitting curves for the original data at each MT station and the response data obtained from the three-dimensional inversion are presented in Figure S1 in the Supplementary Materials.

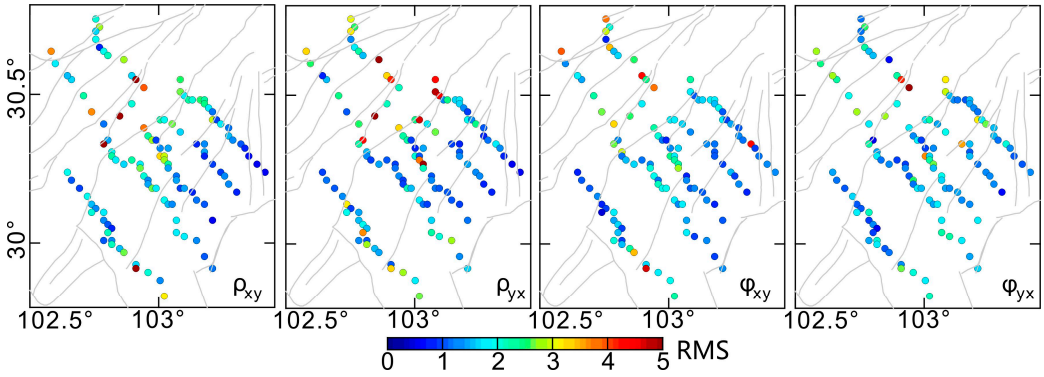

Figure 6. RMS misfit distribution of the 3D inversion.

For certain critical structures within the inversion model, such as C1 in the Lushan earthquake area and C2 beneath the Sichuan Basin, additional tests were conducted. These tests involved altering the resistivity values of these anomalous bodies and subsequently performing forward modeling to assess the changes in the response curves (see Figure S2 in the Supplementary Materials). The results of these tests indicate that the key anomalous bodies within the model are reliable.

Figure 7 presents map views of the deep electrical structure at eight different depths. Centered around the epicenter of the second Lushan earthquake, there exists a high-resistivity body (R1) extending from the shallow crust to the uppermost mantle. The horizontal cross-section of this high-resistivity body is approximately elliptical, with its major axis aligned with the orientation of the LMSFZ (NE direction). The Gengda–Longdong fault constitutes the northwestern boundary of the high-resistivity body, while its southeastern boundary lies in proximity to the SDf. In the depth range greater than 10 km, the high-resistivity body appears relatively continuous. However, within the depth range of less than 10 km, a complex structure characterized by alternating high and low resistivity develops. Particularly, on the southeastern side of the epicenters of the two Lushan earthquakes, the resistivity of the high-resistivity body is notably lower than in other areas, and both the mainshocks and most aftershocks are distributed in this region.

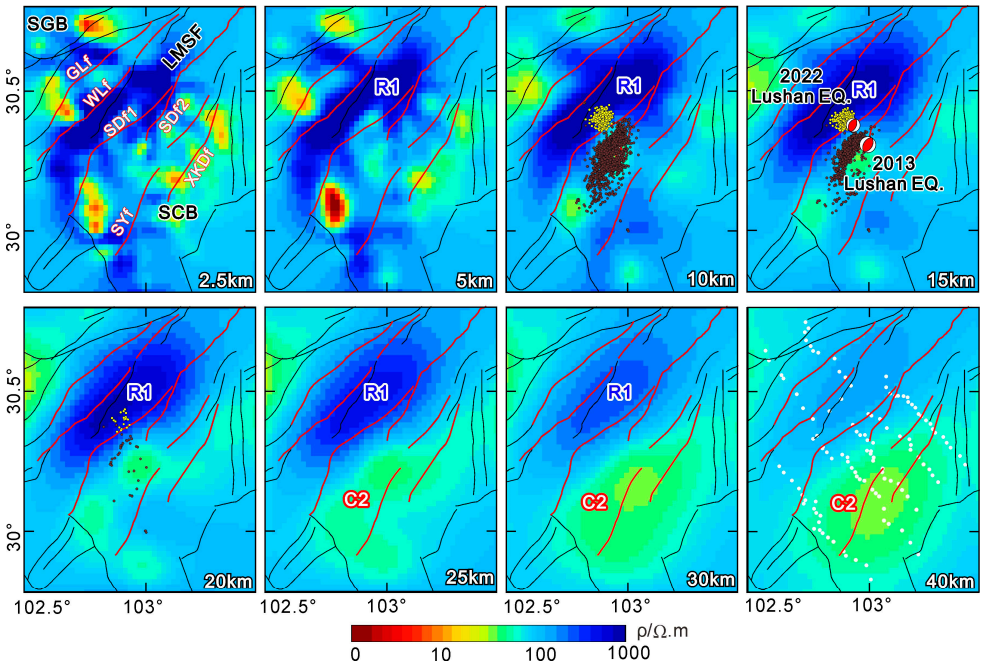

Figure 7. Map view of the 3D inversion model. Red and black lines denote faults.

To the northwest of high-resistivity body R1 lies the Songpan–Ganzi block, where the upper crust exhibits relatively high resistivity within a depth range of approximately 10 km, gradually increasing at greater depths. On the southeastern side of high-resistivity body R1, corresponding to the Sichuan Basin, the resistivity is relatively low from the near surface to several kilometers in depth, generally corresponding to the thickness of sedimentary layers since the Mesozoic. Further depthward, up to approximately 20 km, the resistivity increases again (as shown in Figure 7). Below 20 km, it exhibits relatively low resistivity characteristics.

4. Discussion

4.1. Subsection

Figure 8 presents three-dimensional electrical structure images along five profiles. Among these profiles, BB′ and DD′ are longer and traverse the Songpan–Ganzi block, the LMSFZ, and the Sichuan Basin. AA′, CC′, and EE′ are shorter profiles that do not extend into the Songpan–Ganzi block. The Gengda–Longdong fault is revealed in the BB′ and DD′ profiles as a southwest-dipping boundary with alternating high and low resistivity. The Wulong fault develops within high-resistivity blocks within the Baoxing Complex, with relatively small resistivity variations on both sides. The Shuangshi–Dachuan fault serves as the boundary fault between the LMSFZ and the Sichuan Basin. The resistivity structures along the five profiles indicate that the SDf gradually becomes shallower from southwest to northeast. On the EE′ profile in the southwesternmost region, the SDf appears as a steep electrical boundary extending into the lower crust. On the DD′ and CC′ profiles, the SDf splits into eastern and western branches (SDf1 and SDf2), with SDf1 dipping southeastward and SDf2 showing a slight northwestward dip. They intersect at a depth of approximately 20 km. The CC′ profile, crossing the Lushan earthquake area, exhibits a more prominent Y-shaped electrical discontinuity structure to the east and west of the SDf, with a pronounced difference in electrical properties. On the BB′ and AA′ profiles to the northeast, the electrical discontinuity zone beneath the SDf reaches a depth of only about 5 km. The electrical structure image from the EE′ profile reveals that the Shiyang fault extends to greater depths.

On the southeastern edge of the Songpan–Ganzi block, northwest of the Gengda–Longdong fault, the mid-upper crust exhibits a dual-layered structure of high and low resistivity. In the northwest segment of the DD′ profile, there is evidence of a lower-resistivity layer within the mid-lower crust, extending to several kilometers in depth. This feature is proximal to the deep electrical structure characteristics in the interior of the Songpan–Ganzi block [32,41]. Within the LMSFZ between the Gengda–Longdong fault and the SDf, spanning from near the surface to depths of several tens of kilometers, a high-resistivity body (HRB) is observed, corresponding to the Baoxing Complex. Along the five profiles, it is evident that the southeastern side of the Sichuan Basin, to the southeast of the SDf, generally exhibits alternating high and low resistivity in the upper crust. This corresponds to the complex structural features on Earth's surface, characterized by multiple faults, folds, and anticlines.

At depths of approximately twenty kilometers and deeper, a lower-resistivity body C2 develops in the mid-lower crust, extending shallower to the southwest and deeper to the northeast. The resistivity values also exhibit a southwest-to-northeast gradient, reflecting lower resistivity in the southwest and higher resistivity in the northeast. The longitudinal development of C2 appears as a pocket-like structure with an upper constriction, as evident in profiles CC′, DD′, and EE′ (Figure 7). With increasing depth, C2 extensively extends to the southern region on the southeastern side of the SDf, particularly evident in the southern portion of the BB′ profile (Figure 8).

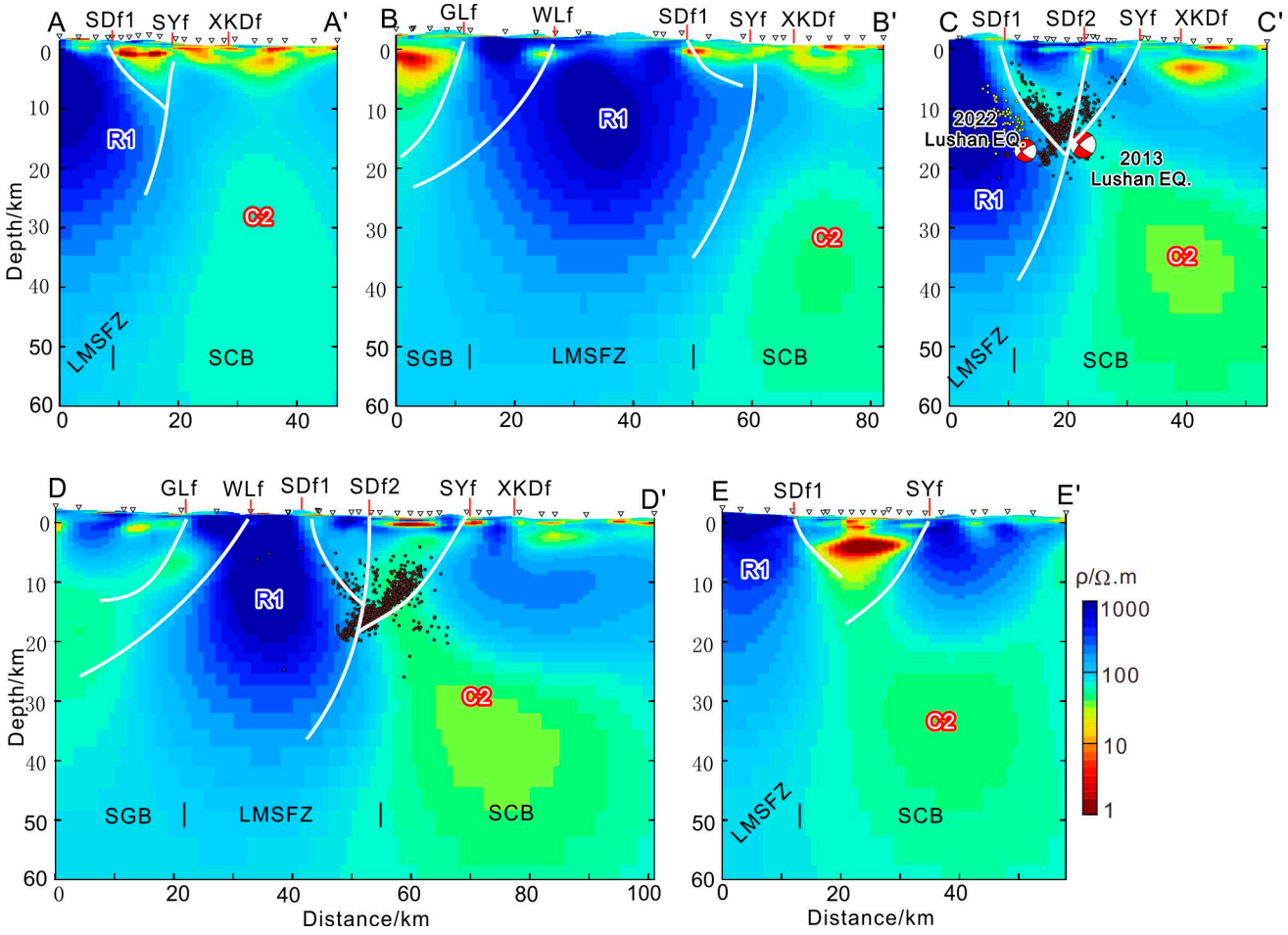

Figure 8. Cross-sections of the 3D inversion model and the interpretations. White lines denote the interpretations of faults. Yellow and brown dots denote aftershocks of the 2013 and 2022 Lushan earthquakes.

4.2. Seismogenic Structure and Environment of Lushan Earthquakes

The electrical structure CC′ profile reveals the SDf separating into western and eastern branches, characterized by contrasting low-resistivity bands. The western branch of the low-resistivity band tilts to the southeast, while the eastern branch is steeper and tilts slightly northwestward. They intersect at a depth of approximately 20 km, forming a Y-shaped configuration (Figure 8). There is a shallow low-resistivity layer in the mid-upper crust. The epicenters of the Lushan earthquakes are situated in the convergence region of the two low-resistivity bands, within the upper constricted region of the pocket-like low-resistivity body (HCL) at depth. The aftershocks of the 2013 Lushan earthquake are distributed along the east–west cross-section, accompanying the Y-shaped low-resistivity band, while the aftershocks of the 2022 Lushan earthquake are distributed along the western boundary of the western branch of the low-resistivity band, with their north–south distribution confined within the region enclosed by the high-resistivity body.

The electrical structure of the crust and upper mantle in the Lushan earthquake area has improved our understanding of the relationships between deep and shallow crustal structures and their connection to seismic activity (Figure 9). The Xinkaidian fault is located at the boundary between the Songpan–Ganzi block (northwest) and the Sichuan Basin (southeast). The Sichuan Basin features extensive Cretaceous strata, while older strata from different geological epochs are exposed in the Songpan–Ganzi uplift, demonstrating that the Songpan–Ganzi block has been tectonically inverted or overthrust above the Sichuan Basin (Figure 2). Correspondingly, the electrical resistivity near the surface in the Songpan–Ganzi block is higher than in the Sichuan Basin. Seismic investigations [45] have

revealed that, from the near surface to a depth of approximately 10 km, Paleozoic strata have developed. Near the southeastern side of the first Lushan earthquake epicenter, a syncline has formed, with its western side corresponding to the Songpan–Ganzi block and its eastern side corresponding to the Sichuan Basin. At depth, beneath the syncline, there is a trough, appearing in a mirror-image relationship, along with variations in the Moho depth and structural discontinuities [21].

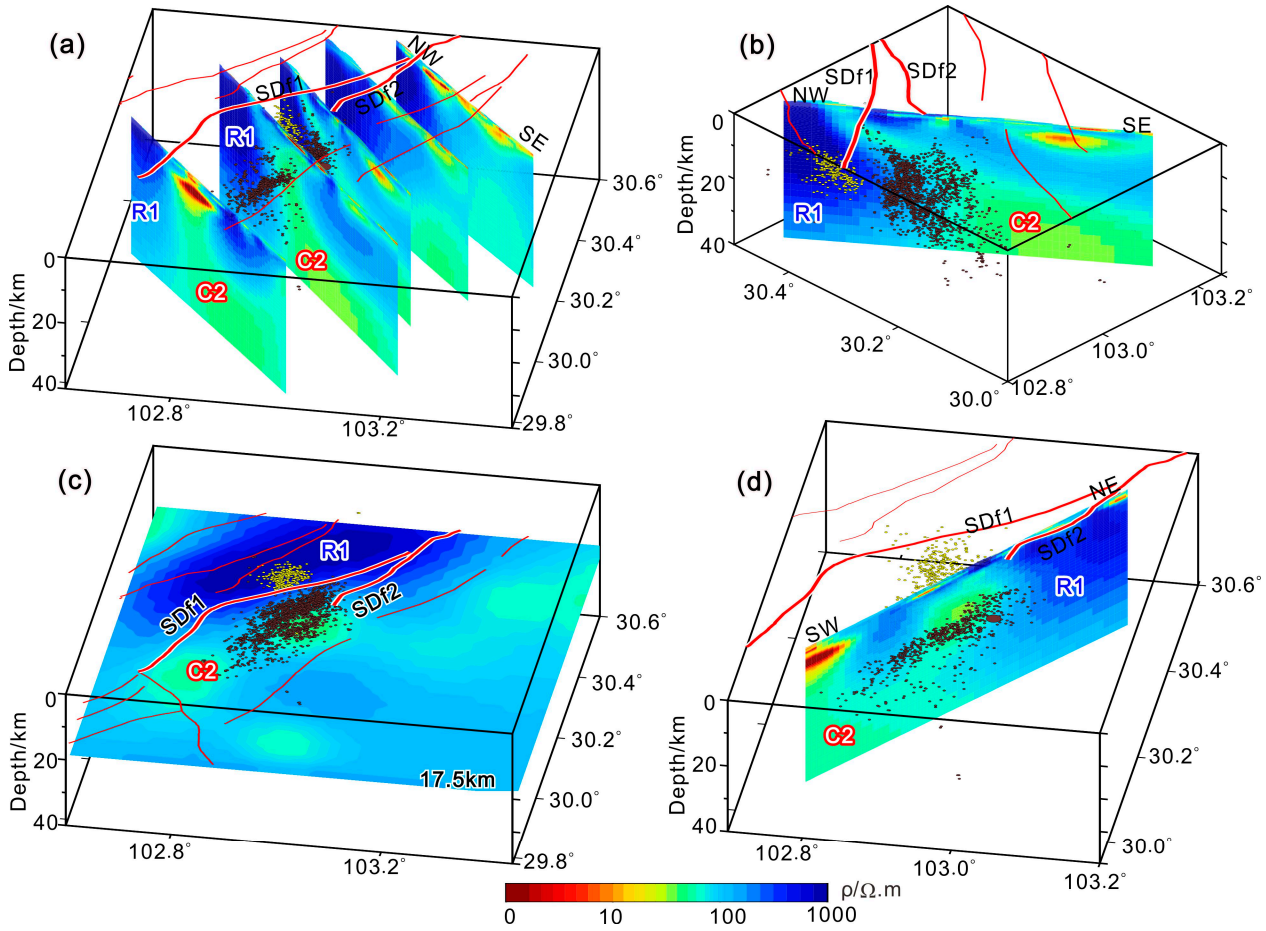

Figure 9. Locations of aftershocks and electrical structure. (**a**) Five NW direction cross-sections of electrical structure. (**b**) A NW direction cross-section of electrical structure. (**c**) Map view for the electrical structure at depth of 17.5 km. (**d**) A NE direction cross-section of electrical structure. Red lines denote faults. Yellow and brown dots denote aftershocks of the 2013 and 2022 Lushan earthquakes.

The 2008 Wenchuan earthquake occurred on the central fault (Yingxiu–Beichuan fault) within the LMSFZ, while the Lushan earthquake took place on the frontal fault (SDf). These two earthquake source areas exhibit entirely different electrical resistivity attributes. The Wenchuan earthquake occurred within a high-resistivity body [41], whereas the Lushan earthquake occurred in an area of transition between high and low resistivity. The rupture of the Wenchuan earthquake is not connected to the rupture of the Lushan earthquake, forming a seismic gap between the Lushan and Wenchuan earthquakes. This seismic gap has shown minimal seismic activity before and after the Wenchuan and Lushan earthquakes [46,47].

Based on results from seismic geology, seismology, and stress measurements, it is suggested that this seismic gap still poses a risk of experiencing moderate to strong earthquakes [32,48–51]. However, seismic tomography results indicate the presence of low-velocity and high-Poisson's-ratio plastic materials beneath the seismic gap, which are unfavorable for strain accumulation. Therefore, the likelihood of a strong earthquake

occurring in this segment is considered low [52,53]. The divergence between these two perspectives may stem from differences in the understanding of the seismogenic environment in the deep region of the earthquake zone and the relationship between material properties and strength.

Deformation observations suggest little post-seismic slip in the southwestern segment of the LMSFZ, indicating possible locking of this segment [54]. MT profiles in the Lushan earthquake area reveal the presence of a high-resistivity medium in the deep portions of the southwestern segment of the LMSFZ. This high-resistivity body corresponds to the inferred locked blocks in the geodetic measurements. Although the Wenchuan and Lushan earthquakes have to some extent released stress along the LMSFZ, this process continues, and seismic activity is related to the accumulation of seismic energy and stress enhancement [55]. Therefore, the seismic hazard of the southwestern segment of the Longmenshan fault zone with deep high-resistivity structures and locking characteristics still deserves attention.

5. Conclusions

Magnetotelluric data were collected from 118 sites in the Lushan earthquake area, and a three-dimensional electromagnetic inversion was performed, taking into account the topography. The three-dimensional electrical structure revealed the Shuangshi–Dachuan fault separating into two distinct low-resistivity bands: a southeastern-dipping low-resistivity band in the western branch and a steeper slightly northwestern-tilted low-resistivity band in the eastern branch. These two branches intersect at a depth of approximately 20 km, forming an extension pattern resembling a Y-shape. The epicenters of the 2013 Lushan M7.0 earthquake and the 2022 Lushan M6.1 earthquake are primarily located in the upper constricted portion of the pocket-like low-resistivity body at depth, where the aftershocks are distributed along the "Y"-shaped low-resistivity body, and their north–south distribution is confined within the region enclosed by the high-resistivity body.

In the region to the southwest and southeast of the Shuangshi–Dachuan fault, deep low-resistivity layers exhibit a tendency to protrude towards shallower depths, as well as towards the northwest and northeast directions. This portrays regional extension movement with stress extending from the southwest to the northeast and from deep to shallow depths. This area is confined by the hard high-resistivity body to the northeast, which facilitated the occurrence of the two Lushan earthquakes. The two Lushan earthquakes and the Wenchuan earthquake occurred in different fault systems within the LMSFZ. The seismic gap characterized by high-resistivity structures, high stress, and locking characteristics between the Lushan earthquake and Wenchuan earthquake areas still warrants attention in terms of seismic hazards.

Supplementary Materials: The following supporting information can be downloaded at https://www.mdpi.com/article/10.3390/rs16020370/s1, Figure S1: Fitting curves of apparent resistivity and phase for the 3D inversion; Figure S2: Model test for C1 and C2.

Author Contributions: Conceptualization, Y.Z., G.Z. and X.S.; formal analysis, L.Z., X.Y., H.Y., X.L. and D.J.; investigation, Y.Z., G.Z. and X.S.; data curation, Y.Z. and L.Z.; writing—original draft preparation, Y.Z., G.Z. and X.S.; writing—review and editing, Y.Z., G.Z. and X.S.; supervision, G.Z.; project administration, Y.Z.; funding acquisition, Y.Z. All authors have read and agreed to the published version of the manuscript.

Funding: This research was funded by the Basic Scientific Funding of the Institute of Geology, China Earthquake Administration, grant number IGCEA1824; the Second Tibetan Plateau Scientific Expedition and Research Program, grant number 2019QZKK0708; State Key Laboratory of Earthquake Dynamics, grant number LED2022B03; the National Natural Science Foundation of China, grant numbers 42204086 and 42174075; the Project of the China Earthquake Administration "Scientific Investigations on the 20 April 2013 Lushan, Sichuan, Earthquake".

Data Availability Statement: Data will be made available on request.

Acknowledgments: We appreciate the Computer Network Information Center at the Institute of Geology, China Earthquake Administration for providing cluster computers used for conducting 3D inversion.

Conflicts of Interest: The authors declare no conflicts of interest.

References

1. Deng, Q.; Chen, S.; Zhao, X. Tectonics, Seismisity and Dynamics of Longmenshan Mountains and Its Adjacent Regions. *Seismol. Geol.* **1994**, *16*, 389–403.
2. Deng, Q.; Zhang, P.; Ran, Y.; Yang, X.; Min, W.; Chu, Q. Basic Features of Active Tectonics in China. *Sci. China (Ser. D)* **2002**, *32*, 1020–1030.
3. Burchfiel, B.C.; Zhiliang, C.; Yupinc, L.; Royden, L.H. Tectonics of the Longmen Shan and Adjacent Regions, Central China. *Int. Geol. Rev.* **1995**, *37*, 661–735. [CrossRef]
4. Zhang, H.; Zhang, P.; Kirby, E.; Yin, J.; Liu, C.; Yu, G. Along-Strike Topographic Variation of the Longmen Shan and Its Significance for Landscape Evolution along the Eastern Tibetan Plateau. *J. Asian Earth Sci.* **2011**, *40*, 855–864. [CrossRef]
5. Zhang, P.-Z.; Wen, X.X.; Shen, Z.-K.; Chen, J.J. Oblique, High-Angle, Listric-Reverse Faulting and Associated Development of Strain: The Wenchuan Earthquake of May 12, 2008, Sichuan, China. *Annu. Rev. Earth Planet Sci.* **2010**, *38*, 353–382. [CrossRef]
6. Wen, X.-Z.; Zhang, P.-Z.; Du, F.; Long, F. The Background of Historical and Modern Seismic Activities of the Occurrence of the 2008 MS8.0 Wenchuan, Sichuan, Earthquake. *Chin. J. Geophys.* **2009**, *52*, 444–454.
7. Wang, W.-M.; Zhao, L.-F.; Li, J.; Yao, Z.-X. Rupture Process of the Ms 8.0 Wenchuan Earthquake of Sichuan, China. *Chin. J. Geophys.* **2008**, *51*, 1403–1410.
8. Xu, X.; Wen, X.; Yu, G.; Chen, G.; Klinger, Y.; Hubbard, J.; Shaw, J. Coseismic Reverse- and Oblique-Slip Surface Faulting Generated by the 2008 Mw 7.9 Wenchuan Earthquake, China. *Geology* **2009**, *37*, 515–518. [CrossRef]
9. Yi, G.-X.; Wen, X.-Z.; Xin, H.; Qiao, H.-Z.; Long, F.; Wang, S.-W. Distributions of Seismicity Parameters and Seismic Apparent Stresses on the Longmenshan-Minshan Tectonic Zone before the 2008 MS8.0 Wenchuan Earthquake. *Chin. J. Geophys.* **2011**, *54*, 1490–1500. [CrossRef]
10. Zhang, P. In-Depth Study of Wenchuan Earthquake, Advancing the Development of Earthquake Science. *Chin. Sci. Bull.* **2018**, *63*, 1862–1863. [CrossRef]
11. Tapponnier, P.; Zhiqin, X.; Roger, F.; Meyer, B.; Arnaud, N.; Wittlinger, G.; Jingsui, Y.; Xu, Z.Q.; Roger, F.; Meyer, B.; et al. Oblique Stepwise Rise and Growth of the Tibet Plateau. *Science* **2001**, *294*, 1671–1677. [CrossRef] [PubMed]
12. Chen, J.; Liu, Q.; Li, S.; Guo, B.; Li, Y.; Wang, J.; Qi, S. Seismotectonic Study by Relocation of the Wenchuan MS8.0 Earthquake Sequence. *Chin. J. Geophys.* **2009**, *52*, 290–297.
13. Fang, L.H.; Wu, J.P.; Wang, W.L.; Lü, Z.Y.; Wang, C.Z.; Yang, T.; Cai, Y. Relocation of the Mainshock and Aftershock Sequences of MS7.0 Sichuan Lushan Earthquake. *Chin. Sci. Bull.* **2013**, *58*, 3451–3459. [CrossRef]
14. Fang, L.; Wu, J.; Wang, W.; Du, W.; Su, J.; Wang, C.; Yang, T.; Cai, Y. Aftershock Observation and Analysis of the 2013 M s 7.0 Lushan Earthquake. *Seismol. Res. Lett.* **2015**, *86*, 1135–1142. [CrossRef]
15. Shen, Z.K.; Sun, J.; Zhang, P.; Wan, Y.; Wang, M.; Bürgmann, R.; Zeng, Y.; Gan, W.; Liao, H.; Wang, Q. Slip Maxima at Fault Junctions and Rupturing of Barriers during the 2008 Wenchuan Earthquake. *Nat. Geosci.* **2009**, *2*, 718–724. [CrossRef]
16. Xu, X.; Wen, X.; Han, Z.; Chen, G.; Li, C.; Zheng, W.; Zhnag, S.; Ren, Z.; Xu, C.; Tan, X.; et al. Lushan M S7.0 Earthquake: A Blind Reserve-Fault Event. *Chin. Sci. Bull.* **2013**, *58*, 3437–3443. [CrossRef]
17. Lu, R.; Xu, X.; He, D.; John, S.; Liu, B.; Wang, F.; Tan, X.; Li, Y. Seismotectonics of the 2013 Lushan Mw 6.7 Earthquake: Inversion Tectonics in the Eastern Margin of the Tibetan Plateau. *Geophys. Res. Lett.* **2017**, *44*, 8236–8243. [CrossRef]
18. Lu, R.; Fang, L.; Guo, Z.; Zhang, J.; Wang, W.; Su, P.; Tao, W.; Sun, X.; Liu, G.; Shan, X.; et al. Detailed Structural Characteristics of the 1 June 2022 MS6.1 Sichuan Lushan Strong Earthquake. *Chin. J. Geophys.* **2022**, *65*, 4299–4310. [CrossRef]
19. Jiang, D.; Zhang, S.; Ding, R. Spatial Pattern of Late Quaternary Shortening Rate in the Longmen Shan Foreland, Eastern Margin of the Tibetan Plateau. *Lithosphere* **2021**, *2021*, 9167174. [CrossRef]
20. Shen, X. An Analysis of the Deformation of the Crust and LAB beneath the Lushan and Wenchuan Earthquakes in Sichuan Province. *Chin. J. Geophys.* **2013**, *56*, 1895–1903. [CrossRef]
21. Wang, F.-Y.; Zhao, C.-B.; Feng, S.-Y.; Ji, J.-F.; Tian, X.-F.; Wei, X.-Q.; Li, Y.-Q.; Li, J.-C.; Hua, X.-S. Seismogenic Structure of the 2013 Lushan MS7.0 Earthquake Revealed by a Deep Seismic Reflection Profile. *Chin. J. Geophys.* **2015**, *58*, 3183–3192. [CrossRef]
22. Feng, Y.-Y.; Yu, C.-Q.; Fan, Z.-G.; Song, L.-R.; Liang, S.-S.; He, J.-J.; Mei, Z.-F. Fine Crustal Structure of the Lushan Area Derived from Seismic Reflection Profiling. *Chin. J. Geophys.* **2016**, *59*, 3248–3259. [CrossRef]
23. He, F.-J.; Liang, C.-T.; Yang, Y.-H.; Fang, L.-H.; Su, J.-R. The Crust Structure of the Unruptured Segment between Wenchuan and Lushan Earthquakes Revealed by Receiver Functions. *Chin. J. Geophys.* **2017**, *60*, 2130–2146. [CrossRef]
24. Huang, Y.; Liang, C.; Wu, J.; Wang, C.; Liu, Z.; Jiang, N. The Seismicity in the Southern Longmenshan Fault Zone Based on a Dense Seismic Array. *Chin. J. Geophys.* **2020**, *63*, 1183–1196. [CrossRef]
25. Liu, Z.; Liang, C.; Hua, Q.; Li, Y.; Yang, Y.; He, F.; Fang, L. The Seismic Potential in the Seismic Gap Between the Wenchuan and Lushan Earthquakes Revealed by the Joint Inversion of Receiver Functions and Ambient Noise Data. *Tectonics* **2018**, *37*, 4226–4238. [CrossRef]

26. Pei, S.; Niu, F.; Ben-Zion, Y.; Sun, Q.; Liu, Y.; Xue, X.; Su, J.; Shao, Z. Seismic Velocity Reduction and Accelerated Recovery Due to Earthquakes on the Longmenshan Fault. *Nat. Geosci.* **2019**, *12*, 387–392. [CrossRef]
27. Cox, S.F. Faulting Processes at High Fluid Pressures: An Example of Fault Valve Behavior from the Wattle Gully Fault, Victoria, Australia. *J. Geophys. Res. Solid Earth* **1995**, *100*, 12841–12859. [CrossRef]
28. Sibson, R.H. Preparation Zones for Large Crustal Earthquakes Consequent on Fault-Valve Action. *Earth Planets Space* **2020**, *72*, 31. [CrossRef]
29. Sibson, R.H. Fault-Valve Behavior and the Hydrostatic-Lithostatic Fluid Pressure Interface. *Earth Sci. Rev.* **1992**, *32*, 141–144. [CrossRef]
30. Karaş, M.; Tank, S.B.; Özaydın, S. Electrical Conductivity of a Locked Fault: Investigation of the Ganos Segment of the North Anatolian Fault Using Three-Dimensional Magnetotellurics. *Earth Planets Space* **2017**, *69*, 107. [CrossRef]
31. Connolly, J.A.D.; Podladchikov, Y.Y. Fluid Flow in Compressive Tectonic Settings: Implications for Midcrustal Seismic Reflectors and Downward Fluid Migration. *J. Geophys. Res. Solid Earth* **2004**, *109*, 1–12. [CrossRef]
32. Zhan, Y.; Zhao, G.Z.; Unsworth, M.; Wang, L.F.; Chen, X.; Li, T.; Xiao, Q.B.; Wang, J.J.; Tang, J.; Cai, J.T.; et al. Deep Structure beneath the Southwestern Section of the Longmenshan Fault Zone and Seimogenetic Context of the 4.20 Lushan MS7.0 Earthquake. *Chin. Sci. Bull.* **2013**, *58*, 3467–3474. [CrossRef]
33. Wang, L.; Zhao, G.; Zhan, Y.; Chen, X.; Xiao, Q.; Zhao, L.; Wang, J.; Qiao, L.; Han, B. Electric Structure of Crust beneath the Southwestern Segment of the Longmenshan Fault Zone. *Seismol. Geol.* **2014**, *36*, 302–311.
34. Wang, X.; Zhang, G.; Zhou, J.; Li, D.; Luo, W.; Hu, Y.; Cai, X.; Guo, Z. Crust and Upper Mantle Electrical Resistivity Structure in the Longmenshan Tectonic Belt and Its Relationship with Wenchuan and Lushan Earthquakes. *Chin. J. Geophys.* **2018**, *61*, 1984–1995. [CrossRef]
35. Wang, M.-M.; Zhan, Y.; Lu, R.-Q.; He, Y.-L.; Zhao, L.-Q.; Sun, X.-Y.; Li, D.-H.; Ma, C. The Seismogenic Structure of the Southern Segment of the Longmen Shan Thrust Belt, Eastern Tibetan Plateau, SW China: A Comprehensive Analysis of Surface Geology and Deep Structure. *J. Asian Earth Sci.* **2019**, *179*, 11–20. [CrossRef]
36. Zhang, G.; Wang, X.; Tang, Y.; Ma, Y.; Zhang, X.; Li, D.; Huang, C.; Cai, X. Three-Dimensional Electrical Structure and Seismogenic Environment of the Crust–Mantle in the Lushan Earthquake Region, China. *Tectonophysics* **2023**, *856*, 229813. [CrossRef]
37. Caldwell, T.G.; Bibby, H.M.; Brown, C. The Magnetotelluric Phase Tensor. *Geophys. J. Int.* **2004**, *158*, 457–469. [CrossRef]
38. Bibby, H.M.; Caldwell, T.G.; Brown, C. Determinable and Non-Determinable Parameters of Galvanic Distortion in Magnetotellurics. *Geophys. J. Int.* **2005**, *163*, 915–930. [CrossRef]
39. Cai, J.; Chen, X.; Xu, X.; Tang, J.; Wang, L.; Guo, C.; Han, B.; Dong, Z. Rupture Mechanism and Seismotectonics of the Ms6.5 Ludian Earthquake Inferred from Three-Dimensional Magnetotelluric Imaging. *Geophys. Res. Lett.* **2017**, *44*, 1275–1285. [CrossRef]
40. Booker, J.R. The Magnetotelluric Phase Tensor: A Critical Review. *Surv. Geophys.* **2014**, *35*, 7–40. [CrossRef]
41. Zhao, G.; Unsworth, M.J.; Zhan, Y.; Wang, L.; Chen, X.; Jones, A.G.; Tang, J.; Xiao, Q.; Wang, J.; Cai, J.; et al. Crustal Structure and Rheology of the Longmenshan and Wenchuan Mw 7.9 Earthquake Epicentral Area from Magnetotelluric Data. *Geology* **2012**, *40*, 1139–1142. [CrossRef]
42. Cheng, Y.; Hu, X.; Han, B.; Li, Y.; Kong, Y.; Tang, J. Magnetotelluric Evidence for Lithospheric Alteration Beneath the Wuyi--Yunkai Orogen: Implications for Thermal Structure of South China. *Geochem. Geophys. Geosyst.* **2022**, *23*, e2022GC010456. [CrossRef]
43. Egbert, G.D.; Kelbert, A. Computational Recipes for Electromagnetic Inverse Problems. *Geophys. J. Int.* **2012**, *189*, 251–267. [CrossRef]
44. Kelbert, A.; Meqbel, N.; Egbert, G.D.; Tandon, K. ModEM: A Modular System for Inversion of Electromagnetic Geophysical Data. *Comput. Geosci.* **2014**, *66*, 40–53. [CrossRef]
45. Wang, M.; Jia, D.; Shaw, J.H.; Hubbard, J.; Plesch, A.; Li, Y.; Liu, B. The 2013 Lushan Earthquake: Implications for Seismic Hazards Posed by the Range Front Blind Thrust in the Sichuan Basin, China. *Geology* **2014**, *42*, 915–918. [CrossRef]
46. Gao, Y.; Wang, Q.; Zhao, B.; Shi, Y. A Rupture Blank Zone in Middle South Part of Longmenshan Faults: Effect after Lushan Ms7.0 Earthquake of 20 April 2013 in Sichuan, China. *Sci. China Earth Sci.* **2014**, *57*, 2036–2044. [CrossRef]
47. Zhao, B.; Gao, Y.; Huang, Z.; Zhao, X.; Li, D. Double Difference Relocation, Focal Mechanism and Stress Inversion of Lushan MS 7.0 Earthquake Sequence. *Chin. J. Geophys.* **2013**, *56*, 3385–3395. [CrossRef]
48. Dong, S.; Han, Z.; An, Y. Paleoseismological Events in the "Seismic Gap" between the 2008 Wenchuan and the 2013 Lushan Earthquakes and Implications for Future Seismic Potential. *J. Asian Earth Sci.* **2017**, *135*, 1–15. [CrossRef]
49. Liu, C.; Zhu, B.; Shi, Y. Do the Two Seismic Gaps in the Southwestern Section of the Longmen Shan Fault Present the Same Seismic Hazard? *J. Geophys. Res. Solid Earth* **2020**, *125*, 1–23. [CrossRef]
50. Guo, R.; Zheng, Y.; Xu, J. Stress Modulation of the Seismic Gap between the 2008 Ms 8.0 Wenchuan Earthquake and the 2013 Ms 7.0 Lushan Earthquake and Implications for Seismic Hazard. *Geophys. J. Int.* **2020**, *221*, 2113–2125. [CrossRef]
51. Li, B.; Xie, F.; Huang, J.; Xu, X.; Guo, Q.; Zhang, G.; Xu, J.; Wang, J.; Jiang, D.; Wang, J.; et al. In Situ Stress State and Seismic Hazard in the Dayi Seismic Gap of the Longmenshan Thrust Belt. *Sci. China Earth Sci.* **2022**, *65*, 1388–1398. [CrossRef]
52. Li, Z.; Tian, B.; Liu, S.; Yang, J. Asperity of the 2013 Lushan Earthquake in the Eastern Margin of Tibetan Plateau from Seismic Tomography and Aftershock Relocation. *Geophys. J. Int.* **2013**, *195*, 2016–2022. [CrossRef]
53. Pei, S.; Zhang, H.; Su, J.; Cui, Z. Ductile Gap between the Wenchuan and Lushan Earthquakes Revealed from the Two-Dimensional Pg Seismic Tomography. *Sci. Rep.* **2014**, *4*, 6489. [CrossRef] [PubMed]

54. Diao, F.; Wang, R.; Wang, Y.; Xiong, X.; Walter, T.R. Fault Behavior and Lower Crustal Rheology Inferred from the First Seven Years of Postseismic GPS Data after the 2008 Wenchuan Earthquake. *Earth Planet Sci. Lett.* **2018**, *495*, 202–212. [CrossRef]
55. Yi, G.-X.; Wen, X.-Z.; Xin, H.; Qiao, H.-Z.; Wang, S.-W.; Gong, Y. Stress State and Major-Earthquake Risk on the Southern Segment of the Longmen Shan Fault Zone. *Chin. J. Geophys.* **2013**, *56*, 1112–1120. [CrossRef]